

# Evaluating the Disentanglement of Deep Generative Models through Manifold Topology

Sharon Zhou, Eric Zelikman, Fred Lu, Andrew Y. Ng, Stefano Ermon  
Stanford University  
{sharonz, ezelikman, fredlu, ang, ermon}@cs.stanford.edu

## Abstract

Learning disentangled representations is regarded as a fundamental task for improving the generalization, robustness, and interpretability of generative models. However, measuring disentanglement has been challenging and inconsistent, often dependent on an ad-hoc external model or specific to a certain dataset. To address this, we present a method for quantifying disentanglement that only uses the generative model, by measuring the topological similarity of conditional submanifolds in the learned representation. This method showcases both unsupervised and supervised variants. To illustrate the effectiveness and applicability of our method, we empirically evaluate several state-of-the-art models across multiple datasets. We find that our method ranks models similarly to existing methods.

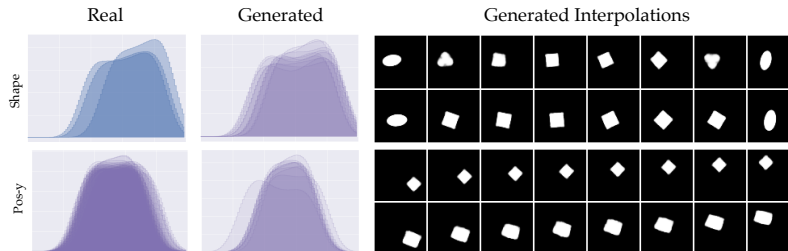


Figure 1: Factors in the *dSprites* dataset displaying topological similarity and semantic correspondence to respective latent dimensions in a disentangled generative model, as shown through Wasserstein RLT distributions of homology and latent interpolations along respective dimensions.

## 1 Introduction

Learning disentangled representations is important for a variety of tasks, including adversarial robustness, generalization to novel tasks, and interpretability [34, 2, 32, 3]. Recently, deep generative models have shown marked improvement in disentanglement across an increasing number of datasets and a variety of training objectives [8, 27, 20, 26, 7, 5, 24]. Nevertheless, quantifying the extent of this disentanglement has remained challenging and inconsistent. As a result, evaluation has often resorted to qualitative inspection for comparisons between models.

Existing evaluation metrics are rigid: while some rely on training additional ad-hoc models that depend on the generative model, such as a classifier, regressor, or an encoder [13, 26, 20, 7, 15, 17, 22, 12], others are tuned for a particular dataset [24]. These both pose problems to the metric’s reliability, its relevance to different models and tasks, and consequently, its applicable scope. Specifically, reliance on training and tuning external models presents a tendency to be sensitive to additional hyperparameters and introduces partiality for models with particular training objectives, e.g. variational

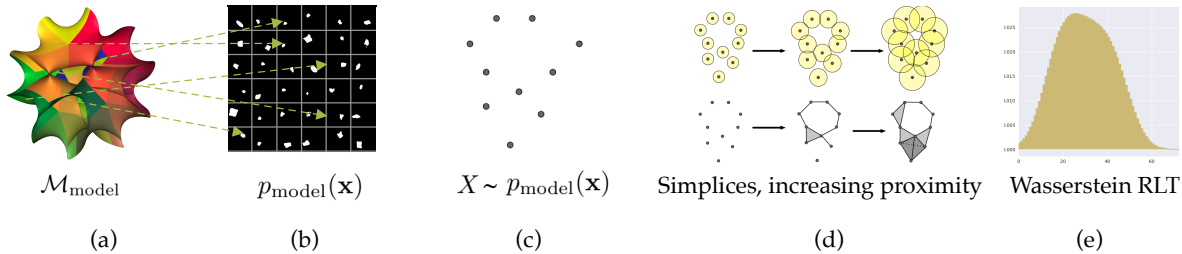


Figure 2: Illustration of obtaining Wasserstein Relative Living Times (W. RLTs) from a manifold. (a) a learned manifold with holes, on which (b)  $p_{\text{model}}(\mathbf{x})$  is presumed to be supported (images here are generated dSprites). From  $p_{\text{model}}(\mathbf{x})$ , we obtain (c) samples  $X$ . From  $X$ , we construct (d) simplicial complexes from increasing the proximity of balls over time, producing a distribution of holes across varying dimensionalities, or an RLT. In this example, we first have no holes in the simplicial complex (homology group  $H_0$ ), then both a 1-dimensional hole and no hole ( $H_1, H_0$ ), and finally only a 1-dimensional hole ( $H_1$ ). Finding the W. barycenter of several RLTs, we obtain (e) a W. RLT.

methods [7, 26, 20, 5] or adversarial methods with an encoder head on the discriminator [8, 27]. In fact, this reliance may provide an explanation for the frequent fluctuation in model rankings when new metrics are introduced [26, 27, 8]. Meanwhile, dataset-specific preprocessing, such as automatically removing background portions from generated portrait images [24], generally limits the scope of the metric’s applicability because it depends on the preprocessing procedure and may otherwise be unreliable without it.

To address this, we introduce an unsupervised disentanglement metric that can be applied across different model architectures and datasets without training an ad-hoc model for evaluation or introducing a dataset-specific preprocessing step. We achieve this by examining topology, an intrinsic property of a manifold that typically exhibits modes corresponding to high-density regions, surrounded by low-density regions [6, 30, 16]. Our method investigates the topology of these low-density regions (holes) by estimating homology, a topological invariant that characterizes the distribution of holes on a manifold. We first condition the manifold on each latent dimension and subsequently measure the homology of these conditional submanifolds. By comparing homology, we examine the degree to which conditional submanifolds continuously deform into each other. This provides a notion of topological similarity that is higher across submanifolds conditioned on disentangled dimensions than those conditioned on entangled ones. From this, we construct our metric using the aggregate topological similarity across data submanifolds conditioned on every latent dimension in the generative model.

In this paper, we make several key contributions:

- We present an unsupervised metric for evaluating disentanglement that only requires the generative model (decoder) and is dataset-agnostic. In order to achieve this, we propose measuring the topology of the learned data manifold with respect to its latent dimensions. Our metric accounts for topological similarity within a dimension and across homologous dimensions.
- We also introduce a supervised variant that compares the generated topology to a real reference.
- For both variants, we develop a topological similarity criterion based on Wasserstein distance.
- Empirically, we perform an extensive set of experiments to demonstrate the applicability of our method across 10 models and three datasets using both the supervised and unsupervised variants. We find that our results are consistent with several existing methods.

## 2 Background

Our method draws inspiration from the Manifold Hypothesis [6, 30, 16], which posits that there exists a low-dimensional manifold  $\mathcal{M}_{\text{data}}$  on which real data lie and  $p_{\text{data}}(\mathbf{x})$  is supported, and that generative models  $g : Z \rightarrow X$  learn an approximation of that manifold  $\mathcal{M}_{\text{model}}$ . As a result, the true data manifold  $\mathcal{M}_{\text{data}}$  contains high-density regions, separated by large expanses of low-density regions, assuming a topology.  $\mathcal{M}_{\text{model}}$  approximates this topology through the learning process.

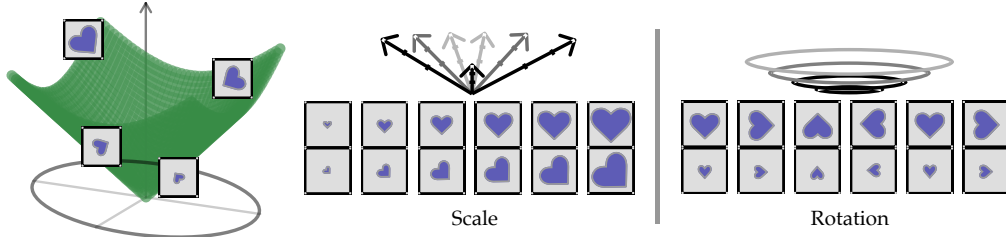


Figure 3: Consider a set of images of a spinning heart with different sizes. We can embed these images on any group which combines a rotational and a scalar invariance (i.e. a group with the  $SO(2,1)$  symmetry), visualizing this as a conical or hemispherical shell. The submanifolds corresponding to a given rotation have no holes, while those corresponding to scale have a 1D hole. Notably, the topology of the submanifold when holding scale fixed is different from the topology when holding rotation fixed. Latent dimensions of a disentangled model would embed images on each axis. By contrast, an entangled model may embed one dimension on an axis and the other in a spiral.

The *topology* of a manifold consists of a set of properties that are invariant to continuous deformations of the manifold, such as bending or stretching, but not to slicing the manifold into submanifolds (subtractive) or joining it with others (additive). These topological properties are *intrinsic* to the manifold, meaning they do not depend on the manifold’s *atlas*. An atlas is a set of *coordinate charts*, or bijective maps, from the manifold to a simpler coordinate space that preserves the manifold’s structure—or, put simply, a parameterization of the manifold. Most manifolds have many possible atlases. For example, it is possible for two generative models  $g$  and  $g'$  to construct the same manifold  $\mathcal{M}_{\text{model}}$ , but have different atlases, or parameterizations  $\{\phi_i : Z \rightarrow X\}$  where  $\phi_i$  is a coordinate chart that is diffeomorphic to  $Z$ .

Among the easiest topological invariants to numerically estimate is homology [19], which characterizes the number of  $k$ -dimensional holes in a topological space such as a manifold. Intuitively, these holes correspond to low-density regions on the manifold. If two manifolds can be continuously deformed into each other, they can be described as *homologous*. Recent work has shown that Relative Living Times (RLTs) [25] offer a computationally efficient method for estimating homology using data samples to approximate the manifold. Under the manifold hypothesis, the latent space of a generative model has an extremely dense underlying manifold with few, if any, holes, making homology difficult to measure and distinguish across submanifolds. As a result, RLTs measure homology on the data manifold. This also enables the direct comparison of generated data manifolds to real ones.

To obtain RLTs, we first construct a family of simplicial complexes—graph-like structures—from data samples, each starting with a set of vertices representing the data points and no edges (see Figure 2). These simplicial complexes topologically approximate the data manifold, by identifying  $k$ -dimensional holes present in the simplices at varying levels of *proximity*. Proximity is defined as the radius of a ball around each symplectic vertex. If the balls of two vertices intersect, an edge is drawn between those vertices. As proximity increases, simplicial complexes with varying numbers of  $k$ -dimensional holes will form—in fact, holes will both appear and disappear as a function of increasing proximity. RLTs use the notion of increasing proximity over time to construct a discrete distribution over the duration of each  $k$ -dimensional hole as it appears and disappears, or their lifetime relative to other holes. The mean of several RLTs produces a discrete probability distribution that estimates the homology of a manifold. This probability distribution is called a Mean Relative Living Time, and the Euclidean distance between two Mean Relative Living Times is used as a measure of topological similarity between data samples, known as the *Geometry Score* [25].

### 3 Manifold Interpretation of Disentanglement

From the manifold perspective, disentanglement is an extrinsic property that is dependent on the generative model’s atlas. Consider a disentangled generative model  $g$  with manifold  $\mathcal{M}$  that assumes topology  $\tau$ . We can define another generative model  $g'$  with the same underlying manifold  $\mathcal{M}$  and  $\tau$ , but it is entangled and has a different atlas. In fact, we can define several alternate disentangled and entangled atlases, provided there are multiple valid factorizations of the space. As a result, we need a method that can detect whether an atlas is disentangled.

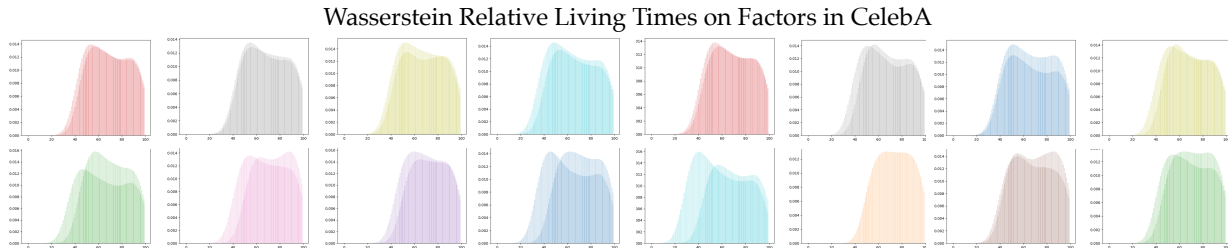


Figure 4: Wasserstein RLTs from several factors in the *CelebA* dataset. Homologous factors are shown on top, and variation from non-homologous candidates below.

In this paper, we slice  $\mathcal{M}$  into submanifolds  $U_{s_i=j} \subset \mathcal{M}$  that are conditioned on a factor  $s_i$  at value  $j$ . These conditional submanifolds have separate topologies from  $\mathcal{M}$  and depend on the coordinate chart  $\phi_i$  associating it with the model’s atlas. If we observe samples from one factor, e.g.  $X_{s_1=j} \sim U_{s_1=j}$  at varying values of  $j$ , we find that all samples  $X_{s_1=j}$  appear identical, except with respect to that single factor of variation  $s_i$  set to a different value of  $j$ . For a generative model, the correspondence between latent dimensions  $z_j$  and factors  $s_i$  is not known upfront. As a result, we perform this procedure by conditioning on each latent dimension  $z_j$ .

**Conditional submanifold topology.** For two submanifolds to have the same topology, there needs to be a continuous deformation from one to the other, i.e. there exists a continuous and invertible mapping between them. First, assume that there exists an invertible mapping, or encoder  $e : X \rightarrow Z$ , and a generative model  $g : Z \rightarrow X$ , where both functions are continuous. Then, for a given  $\mathbf{z}$  and  $\mathbf{x} = g(\mathbf{z})$ , we can recover  $\mathbf{z}$  by composition  $\mathbf{z} = e(g(\mathbf{z}))$ . We can also construct a simple linear mapping  $l : \mathbf{z} \rightarrow \mathbf{z}'$ , which adapts a factor’s value, such that  $\mathbf{z}' = l(e(g(\mathbf{z})))$  remains continuously deformable. This holds across factors, where the manifold is topologically symmetric with respect to different factors, i.e. its conditional submanifolds are homologous. As an example, consider a disentangled generative model  $g(z_0, z_1, z_2)$  that traces a tri-axial ellipsoid  $\frac{x^2}{z_0^2} + \frac{y^2}{z_1^2} + \frac{z^2}{z_2^2} = 1$ . If we condition the model on varying values of each factor, the resulting submanifolds are 2-dimensional ellipses and have the same topology.

Most complex manifolds have submanifolds that are topologically asymmetric between factors. For example, consider a generative model  $g(z_0, z_1)$  that traces a cylindrical shell with angle  $z_0$ , height  $z_1$ , and for simplicity, no thickness. The submanifolds conditioned on angle  $z_0$  form lines (no holes), while the submanifolds conditioned on height  $z_1$  form circles (a 1D hole). However, the topology remains the same for a given factor, e.g. either varying sized lines or circles. Taken together, this means that submanifolds within a factor (intra-factor) are homologous, while submanifolds between factors (extra-factor) can be either homologous or non-homologous.

**Topological asymmetry.** Because topologically asymmetric submanifolds are non-homologous, using a single  $e$  that continuously deforms across submanifolds no longer holds under disentanglement. To address this, assume that for each factor  $j$ , there exists a continuous invertible encoder  $e_j : X \rightarrow Z_j$  that exclusively encodes information on  $j$  from a generated sample. In the cylindrical shell example, this means continuously deforming across submanifolds conditioned on varying values of  $z_0$  using  $e_0$  (deforming between lines) and likewise for  $z_1$  using an  $e_1$  (deforming between circles). Note that this formulation prevents continuous deformations between lines and circles. More generally, we cannot continuously deform across submanifolds conditioned by arbitrary factors and expect the topology to be preserved. This procedure now amounts to performing latent traversals along an axis and observing the topology of the resulting submanifolds. In a disentangled model, the  $j$ -conditional submanifolds exhibit the same topology by continuous composition of  $\mathbf{z} = e_j(g(\mathbf{z}))$ , using a linear mapping that only adapts factor  $j$  across the traversal, i.e.  $\mathbf{z}' = l_j(e_j(g(\mathbf{z})))$ .

In an entangled model by contrast, more than one factor—such as both the angle and height in the cylindrical shell example—exhibit variation along a dimension  $z_j$ . Put another way, the topology on submanifolds conditioned on  $z_j$  changes when multiple factors contribute to variation along this dimension. Concretely, following the cylindrical shell example, a dimension that encodes height and, after a certain height threshold, also begins to adapt the angle will result in a topology that changes at that threshold to include a 2D hole. Consequently, submanifolds conditioned on the same factor  $z_j$  have the same topology in a disentangled model, yet different topology in an entangled one.

Because we cannot assume that the data manifold of a generative model is completely symmetric, we only consider submanifolds to be homologous along the same factor in a disentangled model. By contrast, since these submanifolds are not homologous in an entangled model, we can measure the similarity across these submanifolds to evaluate a model’s disentanglement. Using this notion of intra-factor topological similarity, we may sufficiently measure disentanglement in most cases, but it does not shield us from the scenario where a generative model learns a single trivial factor along all dimensions, i.e. a factorization of one. If we assume that there exists asymmetries in the data manifold, then ensuring that the manifold exhibits topological *dissimilarity* between certain factors would disarm that case. We operationalize this by identifying homologous groups of factors, whereby each group has its own distinct topology to ensure there is not a factorization of one. Within groups, we still measure topological similarity, but between different groups, we also calculate topological dissimilarity. Consequently, topological similarity and dissimilarity form the basis of our metric.

**Ties to prior work.** As noted in a foundational paper on disentanglement [3], disentanglement constitutes a bijective mapping between factors of variation in the data to dimensions in the latent space  $Z$ , e.g.  $\forall_i \mathbf{z}_i = e(g(\mathbf{z}_i))$ . Using homology, we can determine whether this bijective mapping holds along different factors, by observing the topological similarity of their conditional submanifolds and measuring the extent to which they continuously deform into each other. Aligned with newer definitions of disentanglement [21, 12], our framing permits multiple valid factorizations, where different groups of homologous factors can compose alternate factorizations. Our supervised variant is meant to consider a target factorization corresponding to factors on the real manifold. In this variant, we follow the existing definition of supervised disentanglement [33] that allows different subsets of dimensions to contribute to a target factor and for target factors to exhibit statistical dependence.

### 3.1 Topological similarity using Wasserstein Relative Living Times

In order to estimate the topological similarity between conditional submanifolds, we build on Relative Living Times [25] and introduce Wasserstein (W.) Relative Living Times, which accounts for geometric information in the RLTs during aggregation. Instead of assuming Euclidean distances for measuring the mean across RLTs and distances between mean RLTs, we leverage the insight that RLTs themselves are distributions across subsamples and contain useful geometric information that Euclidean distances inherently ignore. Drawing from optimal transport literature, we use the W. barycenter [1] across RLTs in lieu of the Euclidean mean. For distances between W. barycenters, we employ standard W. distance.

In optimal transport, the W. barycenter  $\bar{p}_w$  of the distributions  $p_1 \dots p_N$  intuitively corresponds to finding the minimum cost for transporting  $\bar{p}_w$  to each  $p_i$ , where cost is defined in W-2 distance:

$$\bar{p}_w = \arg \min_q \sum_{j=1}^N \lambda_j W_2^2(q, p_j)$$

where  $\lambda \geq 0$  and  $\sum_{j=0}^N \lambda_j = 1$ . This is a weighted Fréchet mean,  $\bar{p} = \arg \min_q \sum_{j=1}^N \lambda_j d^2(q, p_j)$ , where  $d = W_2^2$ . In contrast, Euclidean distance, or the  $l_2$  norm, is defined using  $d = \|\cdot\|_2^2$ .

Because our distributions represent discrete unnormalized counts of  $k$ -dimensional holes, we leverage recent work in unbalanced optimal transport [9, 14] that assumes that  $p_i$  are not normalized probabilities containing varying cumulative mass. The unbalanced W. barycenter modifies the W. distance to penalize the marginal distributions based on the extended KL divergence [9, 11].

Unlike Euclidean, Hellinger, or total variation distance, W. distance and W. barycenters account for the underlying geometry of distributions. For example, consider a set of two-dimensional distributions  $p_i$  that are merely shifted along one axis from each other, with the same moments except for the first. Using the Euclidean distance to find the average distribution  $\bar{p}$ , for example, would not preserve any moments, only centering the distribution around the desired mean, while the W. barycenter would preserve the second, third, and fourth moments (the shape) and still be centered around the mean.

This distinction is important for our metric, as it affects the preservation of our homology estimates when we aggregate RLT distributions. Put another way, we want our metric to be sensitive not only to the mean of the distribution of holes—i.e. understanding what the average dimensionality of holes are on a submanifold—but also to the shape of the distribution, characterizing the size and number of high-density and low-density regions on each submanifold.

## Spectrally Coclustered Topological Similarity Matrices

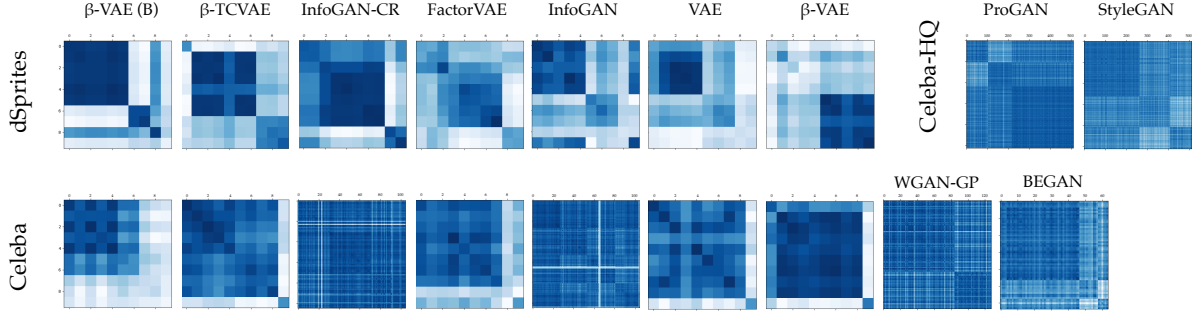


Figure 5: Topological similarity matrices across experimental conditions. Dark clusters along the diagonal indicate homologous groups. Darker values indicate greater similarity (lower  $W.$  distance) to each other. Note that models spectrally cocluster differently across dataset settings.

### 3.2 Metric

Equipped with a procedure for measuring topological similarity, we develop a metric for scoring the disentanglement from intra-group topological similarity and extra-group topological dissimilarity.

Beginning with intra-factor topological similarity, we are concerned with the degree to which the topology of  $p_{\text{model}}(\mathbf{x}|s_i = v)$  varies with respect to a factor  $s_i$  at different values of  $v$ . Specifically, we condition the manifold on a particular factor  $s_i$  at value  $v$ , while allowing other factors  $s_{\setminus i}$  to vary. We then measure the topology of this conditional submanifold. For each factor  $s_i$ , we find the topology of conditional submanifolds at varying values of  $v$ . A disentangled model would exhibit topological similarity within the set of submanifolds conditioned on the same  $s_i$ .

For a generative model, the correspondence between latent dimensions  $z_j$  and factors  $s_i$  is not known upfront. As a result, we perform this procedure by conditioning on each latent dimension  $z_j$ . We then assess pairwise topological similarity across latent dimensions  $\forall_{j,k} \delta(z_j, z_k)$ , using  $W.$  distance between  $W.$  RLTs. This operation constructs a  $j$ -dimensional similarity matrix  $M$ . We use spectral coclustering [10] on  $M$  to cocluster  $z_j$  into  $\xi$  biclusters, which represent different groups of homologous factors. Spectral coclustering uses SVD to identify, in our case, the  $\xi \leq j$  most likely biclusters, or the subsets of rows that are most similar to columns in  $M$ . The resulting biclusters create a correspondence from latent dimensions  $z_i$  to a group of homologous factors  $h_\xi$ . Aggregating biclusters in  $M$ , we obtain a  $\xi$ -dimensional matrix  $M'$  (see examples in Figure 5). We then minimize the total variation of intra-group variance and extra-group variance on  $M'$  to find the value for  $m$ . Using  $M'_\xi$ , we compute a score  $\mu$  that rewards high intra-group similarity  $\rho_\xi = \text{tr}(M')$  and low extra-group similarity  $\rho_{\setminus \xi} = \sum_{a,b} M'_{ab} - \text{tr}(M')$ . This score is based on the normalized cut objective in spectral coclustering to measure the strength of associations within a bicluster [10]. As a result, the unsupervised metric  $\mu = \max_{\xi \in [1,j]} \sum_{\xi} (\rho_\xi - \rho_{\setminus \xi})$ .

**Supervised variant.** In order to capture the correspondence between the learned and real data topology, we present a supervised variant that uses labels of relevant factors on the real dataset to represent the real data topology. While this variant requires labeled data, there are no external ad-hoc classifiers or encoders that might favor one training criterion over another. The real topology is approximated in the same way as the generated, but we have desired groups of factors  $s_i$  upfront. Note that  $s_i$  do not necessarily need to belong to different homology groups; we account for this during spectral coclustering with the generated data manifold. The major difference is that the generated data topology is no longer compared to itself, but to the real data topology, where topological similarity is now computed between the two manifolds:  $\forall_{i,j} \delta(z_j, s_i)$ . Note that the relevant factors in the real topology form a specific factorization, so a model that finds an alternate factorization and that scores well on the unsupervised metric may not fare well on the supervised variant.

We use the same spectral coclustering procedure, though this time on a  $j \times i$  matrix. Note that because it is not a square matrix,  $\rho_\xi = \sum_{a=0}^{\xi} M'_{aa}$  and  $\rho_{\setminus \xi} = \sum_{a=0}^{\xi} \sum_{b=0}^{\xi} M'_{ab} - \rho_\xi$ , where  $\xi = \min(\xi, i)$  so that we only consider the real factors if  $\xi > i$ . Finally, we normalize the final score by the number of factors  $\mu_{\text{SUP}} = \mu/i$ , to penalize methods that do not find any correspondence to some



Table 1: Experimental results on several generative models and dataset settings for our unsupervised  $\mu$  and supervised  $\mu_{\text{SUP}}$  metrics, across five runs. We find that, consistent with other disentanglement metrics, no model architecture that we evaluated supercedes all others on every metric and dataset.

Model	Dataset	$\mu$	$\mu_{\text{SUP}}$	Model	Dataset	$\mu$	$\mu_{\text{SUP}}$
$\beta$ -VAE <sub>B</sub>	dSprites	<b>23.53</b> $\pm$ 8.14	<b>3.55</b> $\pm$ 4.25	$\beta$ -VAE <sub>B</sub>	CelebA	4.73 $\pm$ 2.27	<b>0.29</b> $\pm$ 0.25
$\beta$ -TCVAE	dSprites	14.92 $\pm$ 3.46	-0.79 $\pm$ 1.35	$\beta$ -TCVAE	CelebA	10.66 $\pm$ 2.48	0.04 $\pm$ 0.36
InfoGAN-CR	dSprites	9.73 $\pm$ 4.03	1.85 $\pm$ 2.63	InfoGAN-CR	CelebA	0.72 $\pm$ 0.27	0.07 $\pm$ 0.15
FactorVAE	dSprites	8.66 $\pm$ 1.83	0.35 $\pm$ 0.90	FactorVAE	CelebA	8.53 $\pm$ 4.53	-0.14 $\pm$ 0.28
InfoGAN	dSprites	7.42 $\pm$ 1.19	0.16 $\pm$ 0.92	InfoGAN	CelebA	1.11 $\pm$ 0.81	0.00 $\pm$ 0.01
VAE	dSprites	7.05 $\pm$ 1.25	1.54 $\pm$ 1.27	VAE	CelebA	6.98 $\pm$ 2.78	0.00 $\pm$ 0.15
$\beta$ -VAE	dSprites	6.53 $\pm$ 2.89	1.81 $\pm$ 2.90	$\beta$ -VAE	CelebA	<b>15.10</b> $\pm$ 8.94	0.13 $\pm$ 0.38
StyleGAN	CelebA-HQ	<b>1.03</b> $\pm$ 0.24	<b>0.77</b> $\pm$ 0.07	BEGAN	CelebA	0.85 $\pm$ 0.25	0.22 $\pm$ 0.10
ProGAN	CelebA-HQ	0.68 $\pm$ 0.08	0.37 $\pm$ 0.45	WGAN-GP	CelebA	0.83 $\pm$ 0.29	0.07 $\pm$ 0.13

factors. Ultimately, the supervised score favors groups of latent factors that have similar topological submanifolds to those of the reals.

**Limitations.** In Figure 6, we highlight cases where our metric may face limitations, delineated from scenarios where it would behave as expected. The first limitation is that it is theoretically possible for two factors to be disentangled and, under cases of complete symmetry, still have the same topology. This is more likely in datasets with trivial topologies that are significantly simpler than *dSprites*. While partial symmetry is handled in the metric with spectral coclustering of homologous factors, complete symmetry is not.

Because we assume that the manifold is not perfectly symmetric, we do not account for all factors to present symmetry. In order to safeguard against this case, we would need to consider the covariance of topological similarities across pairwise conditional manifolds. This requires selecting fixed points from  $v$  that hold two dimensions constant, and subsequently verifying that the topologies do not covary. However, this approach comes with a high computational cost for a benefit only to, for the most part, simple toy datasets. If we assign a Dirichlet process prior over all possible topologies [31] and treat the number of factors as the number of samples, we find that the probability of having only a single set of all homologous factors decreases factorially with the number of dimensions  $n$ .

An additional limitation of our method is that RLTs do not compute a full topology of the data manifold, but instead efficiently approximate one topological invariant, homology, so that we can comparatively rank generative models on disentanglement. Our overall approach of measuring disentanglement is general enough to incorporate measurements of other topological invariants.

## 4 Experiments

Across an extensive set of experiments, our goal is to show the extent to which our metric is able to compare across generative model architectures, training criteria (e.g. variational/adversarial, with or without an encoder), and datasets. We additionally show that our metric performs similarly to existing disentanglement metrics.

**Datasets.** We present empirical results on three datasets: (1) *dSprites* [29] is a canonical disentanglement dataset whose five generating factors {shape, scale, orientation, x-position, y-position} are complete and independent, i.e. they fully describe all combinations in the dataset; (2) *CelebA* [28] is a popular dataset for disentanglement and image generation, and is comprised of over 202k human faces, which we align and crop to be  $64 \times 64$  px. There are also 40 attribute labels for each image; and (3) *CelebA-HQ* [23], a higher resolution subset of CelebA consisting of 30,000 images, which has recently gained popularity in image generation [23, 24].

**Generative models.** We compare ten canonical generative models, including a standard VAE,  $\beta$ -VAE [20],  $\beta$ -VAE<sub>B</sub> [5], FactorVAE [26],  $\beta$ -TCVAE [7], InfoGAN [8], InfoGAN-CR [27], BE-

	Similar Topology	Different Topology
Entangled	Expected Low score $\tau$	Not applicable under the manifold interpretation
Disentangled	Unlikely in complex data manifolds	Expected High score $\tau$

Figure 6: Topology-entanglement combinations considered in our method.

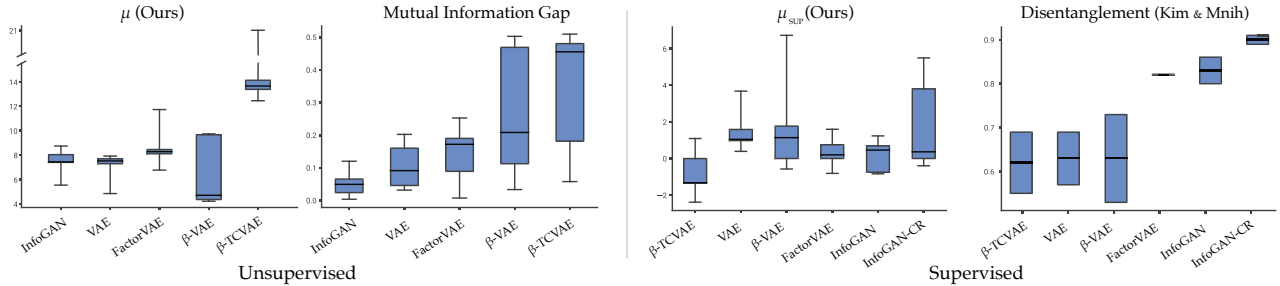


Figure 7: Comparisons of  $\mu$  to MIG [7] and  $\mu_{\text{SUP}}$  to classifier-based disentanglement score [26].

GAN [4], WGAN-GP [18], ProGAN [23], and StyleGAN [24]. We evaluate VAE and InfoGAN variants on dSprites and CelebA, WGAN-GP and BEGAN on CelebA, and ProGAN and StyleGAN on CelebA-HQ. We match models to datasets, on which they have previously demonstrated strong performance and stable training.

**Metric parity.** We find that  $\mu$  and  $\mu_{\text{SUP}}$  rank models similarly to several other frequently cited metrics, including: (1) an information-theoretic metric MIG, which uses an encoder [7], (2) a supervised metric from [26] which uses a classifier, and (3) a dataset-specific metric PPL [24] that caters to high resolution face datasets such as CelebA-HQ. We use scores from their respective papers and prior work [7, 26, 27, 24], and show that our method ranks most or all models the same across each metric ( $\mu$  compared to MIG and PPL,  $\mu_{\text{SUP}}$  to the supervised method). The source of deviation from MIG is the ranking of  $\beta$ -VAE; nevertheless, both of our scores exhibit exceptionally high variance across runs, suggesting that  $\beta$ -VAE has inconsistent disentanglement performance (see Figure 7). The classifier method ranks  $\beta$ -TCVAE and FactorVAE quite far apart, while ours ranks them similarly. We find that their nearly identical training objectives should rank them more closely and do not find this disparity particularly unexpected. Finally, our method agrees with PPL rankings on CelebA-HQ.

As shown in Table 1, these experiments highlight several key observations:

- Performance is not only architecture-dependent, but also dataset-dependent. This highlights the importance of having a metric that can cater to comparisons across these facets. Nevertheless, we note that  $\beta$ -VAE<sub>B</sub> shows especially strong results on both metrics and two dataset settings.
- As expected, the VAE and InfoGAN variants designed for disentanglement show greater performance on  $\mu$  than their GAN counterparts. However, on  $\mu_{\text{SUP}}$ , we find that BEGAN is able to perform inseparably close to  $\beta$ -VAE<sub>B</sub>, suggesting that the model learns dependent factors consistent with the attributes in CelebA.
- With similar training objectives,  $\beta$ -TCVAE and FactorVAE demonstrate comparable strong performances on  $\mu$  across both dSprites and CelebA.  $\beta$ -TCVAE displays slight, yet consistent, improvements over FactorVAE, which may point to FactorVAE’s underestimation of total correlation [7]. Nevertheless, FactorVAE demonstrates higher  $\mu_{\text{SUP}}$  on dSprites.
- StyleGAN demonstrates consistently higher disentanglement, compared to ProGAN, which supports architectural decisions made for StyleGAN [24].

## 5 Conclusion

In this paper, we have introduced a disentanglement metric that measures intrinsic properties of a generative model with respect to its factors of variation. Our metric circumvents the typical requirements of existing metrics, such as requiring an ad-hoc model, a particular dataset, or a canonical factorization. This opens up the stage for broader comparisons across models and datasets. Our contributions also consider several cases of disentanglement, where labeled data is not available (unsupervised) or where direct comparisons to user-specified, semantically interpretable factors are desired (supervised). Ultimately, this work advances our ability to leverage the intrinsic properties of generative models to observe additional desirable facets and to apply these properties to important outstanding problems in the field.



## Broader Impact

This research can aid in alleviating bias in deep generative models and more generally, unsupervised learning. Disentanglement has been shown to help with potentially reducing bias or identifying sources of bias in the underlying data by observing the factors of variation. Those who will benefit from this research will be users of generative models, who wish to disentangle or evaluate the disentanglement of particular models for downstream use. This may include artists or photo editors who use generative models for image editing. For negative consequences, this research broadly advances research in deep generative models, which have been shown to have societal consequences when applied maliciously, e.g. mimicking a political figure in DeepFakes.

## References

- [1] M. Agueh and G. Carlier. Barycenters in the wasserstein space. *SIAM Journal on Mathematical Analysis*, 43(2):904–924, 2011.
- [2] A. A. Alemi, I. Fischer, J. V. Dillon, and K. Murphy. Deep variational information bottleneck. *arXiv preprint arXiv:1612.00410*, 2016.
- [3] Y. Bengio, A. Courville, and P. Vincent. Representation learning: A review and new perspectives. *IEEE transactions on pattern analysis and machine intelligence*, 35(8):1798–1828, 2013.
- [4] D. Berthelot, T. Schumm, and L. Metz. Began: boundary equilibrium generative adversarial networks. *arXiv preprint arXiv:1703.10717*, 2017.
- [5] C. P. Burgess, I. Higgins, A. Pal, L. Matthey, N. Watters, G. Desjardins, and A. Lerchner. Understanding disentangling in beta-vae. *arXiv preprint arXiv:1804.03599*, 2018.
- [6] L. Cayton. Algorithms for manifold learning. *Univ. of California at San Diego Tech. Rep*, 12(1-17):1, 2005.
- [7] T. Q. Chen, X. Li, R. B. Grosse, and D. K. Duvenaud. Isolating sources of disentanglement in variational autoencoders. In *Advances in Neural Information Processing Systems*, pages 2610–2620, 2018.
- [8] X. Chen, Y. Duan, R. Houthoofd, J. Schulman, I. Sutskever, and P. Abbeel. Infogan: Interpretable representation learning by information maximizing generative adversarial nets. In *Advances in neural information processing systems*, pages 2172–2180, 2016.
- [9] L. Chizat, G. Peyré, B. Schmitzer, and F.-X. Vialard. Scaling algorithms for unbalanced optimal transport problems. *Mathematics of Computation*, 87(314):2563–2609, 2018.
- [10] I. S. Dhillon. Co-clustering documents and words using bipartite spectral graph partitioning. In *Proceedings of the seventh ACM SIGKDD international conference on Knowledge discovery and data mining*, pages 269–274, 2001.
- [11] P. Dognin, I. Melnyk, Y. Mroueh, J. Ross, C. D. Santos, and T. Sercu. Wasserstein barycenter model ensembling. *arXiv preprint arXiv:1902.04999*, 2019.
- [12] S. Duan, L. Matthey, A. Saraiva, N. Watters, C. P. Burgess, A. Lerchner, and I. Higgins. Unsupervised model selection for variational disentangled representation learning. *arXiv preprint arXiv:1905.12614*, 2019.
- [13] C. Eastwood and C. K. Williams. A framework for the quantitative evaluation of disentangled representations. 2018.
- [14] C. Frogner, C. Zhang, H. Mobahi, M. Araya, and T. A. Poggio. Learning with a wasserstein loss. In *Advances in Neural Information Processing Systems*, pages 2053–2061, 2015.
- [15] X. Glorot, A. Bordes, and Y. Bengio. Domain adaptation for large-scale sentiment classification: A deep learning approach. 2011.
- [16] I. Goodfellow, Y. Bengio, and A. Courville. *Deep learning*. MIT press, 2016.

- [17] W. Grathwohl and A. Wilson. Disentangling space and time in video with hierarchical variational auto-encoders. *arXiv preprint arXiv:1612.04440*, 2016.
- [18] I. Gulrajani, F. Ahmed, M. Arjovsky, V. Dumoulin, and A. C. Courville. Improved training of wasserstein gans. In *Advances in Neural Information Processing Systems*, pages 5767–5777, 2017.
- [19] A. Hatcher. *Algebraic topology*. Cambridge University Press, 2005.
- [20] I. Higgins, L. Matthey, A. Pal, C. Burgess, X. Glorot, M. Botvinick, S. Mohamed, and A. Lerchner. beta-vae: Learning basic visual concepts with a constrained variational framework. *Iclr*, 2(5):6, 2017.
- [21] I. Higgins, D. Amos, D. Pfau, S. Racaniere, L. Matthey, D. Rezende, and A. Lerchner. Towards a definition of disentangled representations. *arXiv preprint arXiv:1812.02230*, 2018.
- [22] T. Karaletsos, S. Belongie, and G. Rätsch. Bayesian representation learning with oracle constraints. *arXiv preprint arXiv:1506.05011*, 2015.
- [23] T. Karras, T. Aila, S. Laine, and J. Lehtinen. Progressive growing of gans for improved quality, stability, and variation. *arXiv preprint arXiv:1710.10196*, 2017.
- [24] T. Karras, S. Laine, and T. Aila. A style-based generator architecture for generative adversarial networks. *arXiv preprint arXiv:1812.04948*, 2018.
- [25] V. Khruikov and I. Oseledets. Geometry score: A method for comparing generative adversarial networks. *arXiv preprint arXiv:1802.02664*, 2018.
- [26] H. Kim and A. Mnih. Disentangling by factorising. *arXiv preprint arXiv:1802.05983*, 2018.
- [27] Z. Lin, K. K. Thekumparampil, G. Fanti, and S. Oh. Infogan-cr: Disentangling generative adversarial networks with contrastive regularizers. *arXiv preprint arXiv:1906.06034*, 2019.
- [28] Z. Liu, P. Luo, X. Wang, and X. Tang. Deep learning face attributes in the wild. In *Proceedings of International Conference on Computer Vision (ICCV)*, 2015.
- [29] L. Matthey, I. Higgins, D. Hassabis, and A. Lerchner. dsprites: Disentanglement testing sprites dataset. <https://github.com/deepmind/dsprites-dataset/>, 2017.
- [30] H. Narayanan and S. Mitter. Sample complexity of testing the manifold hypothesis. In *Advances in neural information processing systems*, pages 1786–1794, 2010.
- [31] A. Ranganathan. *Probabilistic topological maps*. PhD thesis, Georgia Institute of Technology, 2008.
- [32] K. Ridgeway. A survey of inductive biases for factorial representation-learning. *arXiv preprint arXiv:1612.05299*, 2016.
- [33] R. Shu, Y. Chen, A. Kumar, S. Ermon, and B. Poole. Weakly supervised disentanglement with guarantees. *arXiv preprint arXiv:1910.09772*, 2019.
- [34] D. Stutz, M. Hein, and B. Schiele. Disentangling adversarial robustness and generalization. In *Proceedings of the IEEE Conference on Computer Vision and Pattern Recognition*, pages 6976–6987, 2019.